Numerical modeling of the impact of geometry and wall components on transport in the tokamak edge

Eric Serre, Hugo Bufferand, A. Paredes, Frédéric Schwander, Guido Ciraolo, Philippe Ghendrih, Patrick Tamain

Numerical Modeling of the Impact of Geometry and Wall Components on Transport in the Tokamak Edge

E. Serre[*1], **H. Bufferand**[1], **A. Paredes**[1], **F. Schwander**[1], **G. Ciraolo**[1], **Ph. Ghendrih**[2], and **P. Tamain**[2]

[1] M2P2 UMR 6181, CNRS - Aix-Marseille Université, France
[2] CEA Cadarache, IRFM, Saint Paul-Lez-Durance, France

The SOLEDGE suite of codes has been specially designed to model the transition region from the hot core plasma to the first wall of tokamak, through the Last Closed Flux Surface (LCFS). It is designed to model electrostatic fluid turbulence for an isothermal plasma or for a plasma with temperature variations. Dedicated discretization algorithms have been implemented to handle equations for ion density, electron/ion temperatures and parallel momentum, both for the realistic cross-section of a diverted tokamak and for a three-dimensional cylindrical annulus. The efficient penalization method introduced in Ref. [5] has been implemented, allowing straightforward handling of solid obstacles by treating them as sink regions corresponding to strong plasma recombination in the solid state material. The SOLEDGE capability is exemplified here by simulating two equilibria: (i) a 3D cylindrical annulus and (ii) the cross-section of a diverted tokamak. In the annulus, the analysis of the impact of a secondary discrete limiter shows that the toroidal symmetry usually assumed for density and Mach profiles is broken. The density exhibits significant variations in the toroidal direction that extend over a large region of the scrape-off layer where magnetic field lines are connected to a secondary limiter. In the diverted geometry, computations show a transition from subsonic to supersonic flow in the vicinity of the X-point that is related to the location of particle sources and sinks between the edge connected region and the divertor region.

Key words Plasma transport simulation, fluid equations, plasma equilibriums, secondary limiter.

1 Introduction

Tokamak performance is strongly dependent on the flows in the edge plasma,the transition region across the separatrix from the hot core plasma to the first wall. Transport properties in this region are a fundamental player in edge physics and affect both core plasma confinement and plasma wall interactions. The difficulty in simulating the plasma boundary region is mainly due to the transition from closed to open magnetic flux surfaces and the the presence of X-points or limiters involving sheath physics in the Scrape-Off-Layer (SOL). Thus, simulations at the edge are challenging and require specific algorithms. With the recent development of the family of three-dimensional nonlinear codes SOLEDGE, simulations at the edge have just begun both in circular [8] and diverted geometries. The codes solve the fluid equations within the drift approximation. Five equations can be derived for plasma density, parallel momentum, electron and ion temperatures and electrostatic potential. The validation of the codes and the models have begun in transport regimes using anomalous diffusion. Results have been benchmarked with analytical predictions and experimental measurements in Tore Supra [2, 7].

The volume penalization proposed in Ref. [5] for a reduced model of transport equations for the ion density and the particle flux in the direction parallel to the magnetic field is attractive for representing plasma facing components. Solid obstacles are treated as a region of the plasma governed by a very strong particle sink corresponding to strong plasma recombination at the solid state material. The plasma-limiter interaction is then no longer treated by imposing Bohm conditions on the obstacle surface but by adding penalization terms to conservation equations, characterized by a mask function over the obstacle in which density and parallel momentum are penalized toward zero. Consequently, Cartesian grids can be used in the now obstacle-free domain, and

* Corresponding author: E-mail: eric.serre@L3m.univ-mrs.fr, Phone: +00 33 4 91 11 85 35, Fax: +00 33 4 91 11 85 02

modification of the obstacle location and geometry becomes straightforward Although the main plasma facing components, such as divertor plates or limiters, exhibit near-invariance in the toroidal direction in relatively standard geometries, one also finds a large variety of secondary limiters that affect the transport properties and flow structure in the SOL. Thus, the code capability is first exemplified by showing the impact of a discrete 3D limiter on density and parallel momentum, for an isothermal plasma in a circular geometry (Sec. 3). Such results can help to interpret probe flow measurements made in a series of experiments dedicated to the determination of a quantitative characterization of the radial flux that enters the SOL [2]. The knowledge of Mach number maps is of interest in the investigation of divertor plasma physics because this parameter can be used to determine the location of the ionization front at the subsonic-supersonic transition [4]. In Sec. 4, a plasma equilibrium in a diverted tokamak that shows a transition from subsonic to supersonic flow in the vicinity of X-point is simulated and analyzed.

2 Fluid modeling

The geometrical domain can be a circular annulus or the cross-section of a diverted tokamak. It spans the Last Closed Flux Surface (LCFS) and extends up to the tokamak wall, requiring boundary conditions for open field lines. Consider the curvilinear coordinates (ψ, θ, φ) based on the poloidal magnetic flux ψ, the poloidal angle θ and the toroidal angle φ. The magnetic field $\vec{B}$ is assumed to be steady in time. The constant ψ surfaces are tangential to $\vec{B}$, a sum of two non-zero components B_θ and B_ϕ. The quasi-neutral plasma is modeled as an isothermal compressible fluid for which the density field N, the momentum field Γ projected along the magnetic field direction, and the associated Mach number M=Γ/N satisfy the system of dimensionless conservation laws for both geometries:

$$\partial_t N + \nabla_\parallel \Gamma - D\nabla_\perp^2 N = 0, \tag{1}$$

$$\partial_t \Gamma + \nabla_\parallel \left(\frac{\Gamma^2}{N} + N \right) - \nu \nabla_\perp^2 \Gamma = 0, \tag{2}$$

where D and ν correspond to effective particle and momentum diffusivities, respectively. The operator $\nabla_\parallel$ is the projection of the gradient along the magnetic field defined as $(\vec{B} \cdot \nabla)/|\vec{B}|$, and $\nabla_\perp$ is its projection in the perpendicular plane defines as $(\nabla - \nabla_\parallel)$. In the diverted geometry, the equations are written assuming toroidal symmetry in a curvilinear system of coordinates (ψ, θ, φ) where the metric coefficients are computed from the magnetic equilibrium provided by a Grad-Shafranov solver.

Boundary conditions-No-flux boundary conditions are imposed for both density and momentum on the tokamak wall of the domain, $\partial_n N = \partial_n \Gamma = 0$, n being the normal to the wall. On the inner boundary (at the core), a finite negative density gradient is imposed to ensure a steady fueling of plasma and to compensate for losses on the sides of the limiter, $\partial_n N = -Q$. The parallel momentum is fixed at the core by imposing a parallel velocity, here chosen to be $M = 0$. At the divertor plates, the density flux is free and Bohm boundary conditions are enforced according to standard sheath theory (the Mach number M satisfies $|\mathrm{M}| = 1$ with plasma flow directed towards the limiter) , so that both density and momentum are absorbed by the limiter.

Numerics-The tokamak cross-section is discretized using a second-order finite-difference scheme on a Cartesian grid. Time advance is performed using a second order implicit-explicit scheme, where the parallel direction is treated with a second-order ENO reconstruction scheme, adequate for the high Mach numbers encountered while reasonably accurate and, in particular, less dissipative than equivalent order TVD schemes. Global second order accuracy in time and space is thus achieved. A domain decomposition technique is used to map the diverted cross-section into a set of Cartesian subdomains as illustrated on Fig. 1. The domain decomposition is performed in order to allow only one neighbor per side of each subdomain, each subdomain being associated to a processor using the OpenMP library. The explicit treatment of the boundary conditions at the interfaces ensures C^1-continuity of the solution between the domain.

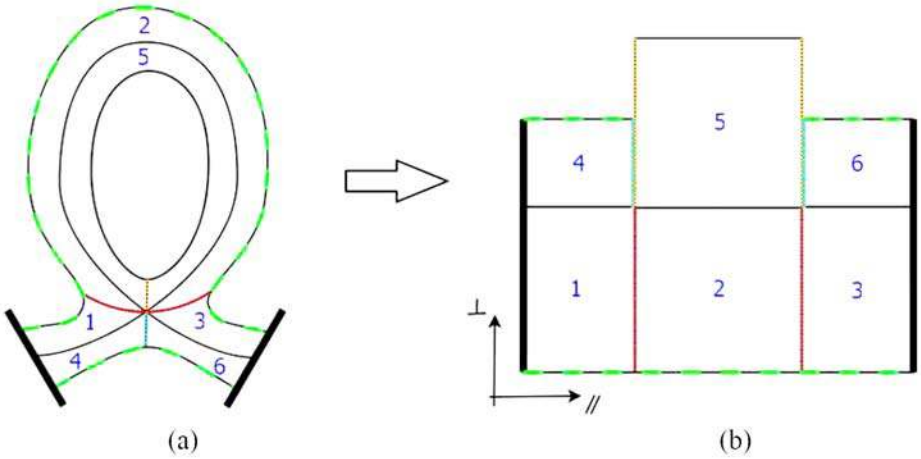

Fig. 1 Domain decomposition of the diverted cross-section and mapping onto a Cartesian domain. The SOL region is decomposed in regions 1, 2 and 3. Regions 4 and 6 correspond to the private region and region 5 to the edge. One notices that areas 4 and 6 are connected but have no direct connection with area 5. Area 5 is periodic in the parallel direction.

3 Impact of a secondary limiter on a (N, Γ)-equilibrium in a circular annulus

The technique introduced in Isoardi *et al.* [5] is extended here to model 3D obstacles in a circular annulus. Contrary to the case of the axisymmetric limiter, the plasma impacts the limiter on poloidally as well as toroidally facing sides. Limiters are introduced in the previous system of Equations (1) and (2) through two terms (discretized implicitly in time) which bring density and momentum close to zero inside the limiter.

$$\partial_t N + \nabla_\parallel \Gamma + \underbrace{\frac{\chi}{\eta}\left(N - N_\Omega\right)}_{\text{Density penalization}} - D\nabla_\perp^2 N = 0, \tag{3}$$

$$\partial_t \Gamma + \nabla_\parallel \left(\frac{\Gamma^2}{N} + N\right) + \underbrace{\frac{\chi}{\eta}\left(\Gamma - N M_\Omega\right)}_{\text{Momentum penalization}} - \nu\nabla_\perp^2 \Gamma = 0 \tag{4}$$

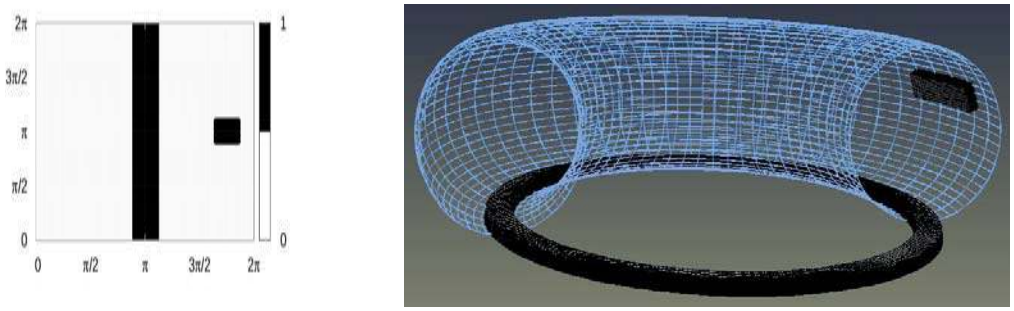

Fig. 2 Cylindrical annular configuration of aspect ratio $\epsilon = 3$ (Tore Supra) with one main toroidally symmetric limiter and a secondary limiter modeled by penalization. (a) Map of the mask function χ, with white regions ($\chi = 1$) showing the localization of solid obstacles). The horizontal and vertical axis show the poloidal and the toroidal angle respectively. (b) Mesh distribution on the torus and on the limiters.

The characteristic function χ carries the information of limiter localization (see Fig. 2(a)). It takes the value 1 inside a limiter and 0 outside. Inside a limiter, the density is fixed to a nearly zero value (here $N_\Omega = 10^{-7}$) to avoid spurious numerical oscillations within the obstacle and the Mach number profile is fixed via M_Ω. The

penalization parameter η is taken as small as possible, here $\eta < 10^{-7}$. The safety factor q, which defines the magnetic field direction, is assumed to have a quadratic profile in minor radius r. Effective particle and momentum diffusivities D and ν are assumed to be equal and fixed at 10^{-5}.

A secondary discrete limiter centered at $\theta = 23\pi/18$ and $\varphi = \pi$ is added to the toroidal one as shown in Fig. 2. Density and parallel Mach maps in the (θ, φ)-plane are shown in Fig. 3(a). It is worthwhile noting that the Bohm condition (Mach=$\pm$1) at the poloidal surface of the 3D limiter is still verified, as previously observed for axisymmetric limiters [5]. Results show that the non-axisymmetric limiter, though small in size, markedly breaks the poloidal symmetry with respect to the main limiter. Moreover, strong variations of density are observed in the toroidal direction, as can be seen in the profile on Fig. 3 (b) which crosses the non-axisymmetric limiter. At the same poloidal angle ($\theta = 23\pi/18$), ($N_{max}/N_{min} \approx 4$). The density map shows that the disturbed region, characterized by a low density, is not restricted around the secondary limiter, but extends to the whole SOL region connected to the secondary limiter by magnetic field lines.

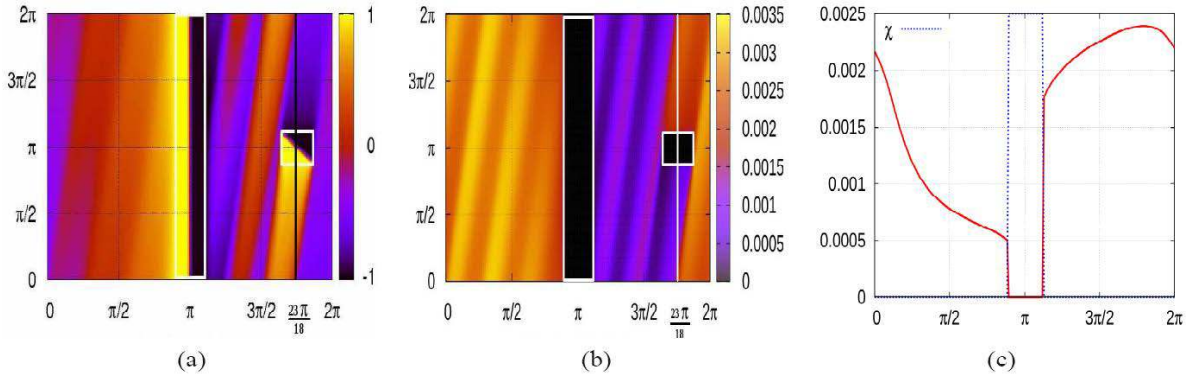

Fig. 3 Plasma equilibrium in a cylindrical annulus with a main, axisymmetric limiter and a secondary, discrete limiter. Maps in the (θ, φ)-plane of (a) the Mach number and (b) the plasma density. The horizontal and vertical axis show the toroidal and the poloidal angle, respectively. (c) Toroidal profile of density at $\theta = 23\pi/8$. $D = \nu = 10^{-5}$.

4 Transition from subsonic to supersonic flow in the vicinity of the X-point

A 2D (N, Γ)-equilibrium is calculated in the cross-section of the diverted geometry of ITER (Figure 4). The Bohm condition is applied on the divertor plates (no penalization). A map of the parallel Mach number is plotted in the cross section on Fig. 4 (left). A transition from subsonic to supersonic flow ($|M| \approx 3$) is observed in the SOL in the neighborhood of the X-point. Such behavior can be understood through an analogy with fluid mechanics, by analyzing the well-known flow of a compressible fluid in a convergent-divergent nozzle. Indeed, consider a tube in which the parallel flow is constant: in the edge connected region, the parallel momentum increases due to the flux of particles coming from the core (source), corresponding to a decrease of the tube corss-section. On the contrary, in the divertor region, the action of the divertor plates as sinks and, combined with the perpendicular diffusive transport on both sides of the field line, imply a decrease of the parallel momentum analogous to an increase of the tube cross-section. Following the theoretical analysis presented in Ref. [3], such a transition can be investigated using a single control parameter A, the ratio of the particle flux multiplied by the acoustic velocity to the total momentum flux (or total plasma pressure), $A = 2\Gamma m_i c_s/\Pi$. Indeed, without loss of generality, Eqs. (1, 2) can be rewritten as steady state equations:

$$\partial_s \Gamma = S_N, \tag{5}$$

$$\frac{1}{m_i}\partial_s \Pi = S_\Gamma. \tag{6}$$

with new source terms for particles and momentum S_N and S_Γ, where the direction of interest is aligned along the plasma flow and is labeled by the curvilinear coordinate s. Combining the above equations, the Mach number and density are obtained as roots of second-order polynomials and as a functions of a unique control parameter A that is a nonlinear function of the Mach number, $A = 2M/(1+M^2)$, bounded between -1 and 1. By definition of

A, the transition to a supersonic regime requires $dA/dM = 0$. In particular, for a continuous transition along the field line a necessary condition is $\partial_s A = 0$. To be sufficient, the sign of $\partial_s A$ must change. In the sheath-limited regime, the field line is isothermal and if one assumes negligible momentum loss ($S_\Gamma \approx 0$), the variation of $\partial_s A$ is given by:

$$\frac{1}{A}\partial_s A = \frac{1}{\Gamma}\partial_s \Gamma \Rightarrow \partial_s A = \frac{2m_i c_s}{\Pi}\partial_s \Gamma. \tag{7}$$

The transition to the supersonic regime can then only take place in the vicinity of the point where $\partial_s \Gamma = 0$ (see Fig. 4(c)). According to Eq. 1, this is the exact transition point in steady state if there is a transition from a positive to a negative particle source, as occurs where the radial density profile changes convexity.

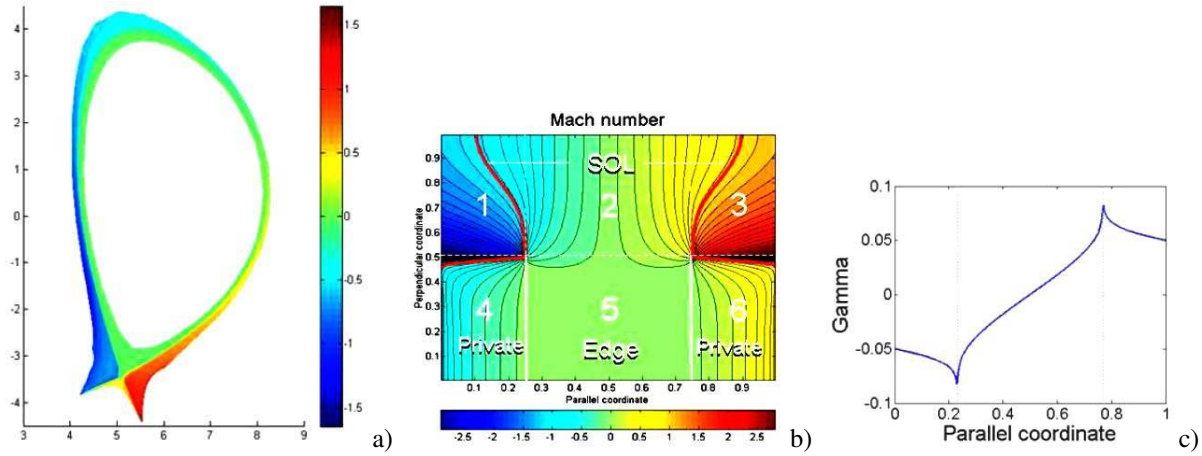

Fig. 4 Plasma equilibrium in the cross-section of a diverted tokamak (ITER). (a) and (b) are maps of the parallel Mach number showing the subsonic-supersonic transition. (c) The the parallel profile of Γ showing the change in the sign of the derivative corresponding to the location of the transition.

5 Concluding remarks

The SOLEDGE suite of code has been designed to solve a fluid model for boundary plasmas in flexible geometries. The computational domain includes the LCFS and the outer part of the closed flux region, the SOL and the private flux region. It can be run in transport regimes for anomalous diffusion and, in the near future, for fully established turbulence.

Acknowledgements This work was granted access to the HPC resources of IDRIS under the allocation 2011-0242 made by GENCI (Grand Equipement National de Calcul Intensif). Financial support from ANR is also acknowledged, project ANR-09-BLAN-0035-01.

References

[1] H. Bufferand, et al., J. Nucl. Mater. **415**, 589 (2011).
[2] N. Fedorczak, et al., J. Nucl. Mater. **229**, 2220 (2010).
[3] Ph. Ghendrih, et al., Plasma Phys. Control. Fusion **53**, 054019 (2011).
[4] Ph. Ghendrih, Phys. Plasmas **1**, 1929 (1994).
[5] L. Isoardi, et al., J. Comp. Phys. **229**, 2220 (2009).
[6] A. Paredes, et al., J. Nucl. Mater. **415**, 579 (2011).
[7] G. Dif-Pradalier, et al., J. Nucl. Mater. **415**, 597 (2011).
[8] F. Schwander, et al., J. Nucl. Mater. **415**, 601 (2011).